Oxidation State Distributions Provide Insight into Parameters Directing the Assembly of Metal-Organic Nanocapsules

Oxidation State Distributions Provide Insight into Parameters Directing the Assembly of Metal-Organic Nanocapsules

Asanka S. Rathnayake,[†] Hector W. L. Fraser,[‡] Euan K. Brechin,[‡] Scott J. Dalgarno,[§] Jakob E. Baumeister,[†] Pokpong Rungthanaphatsophon,[†] Justin R. Walensky,[†] Charles L. Barnes,[†] and Jerry L. Atwood.[*†]

[†]Department of Chemistry, University of Missouri, 601, S. College Avenue, Columbia, MO 65211 (USA)

[‡]EaStCHEM School of Chemistry, The University of Edinburgh, David Brewster Road, EH9 3FJ, Edinburgh (UK)

[§]Institute of Chemical Sciences, Heriot-Watt University, Riccarton, Edinburgh, EH14 4AS (UK)

ABSTRACT: Two structurally analogous Mn-seamed *C*-alkylpyrogallol[4]arene (PgC_n)-based metal-organic nanocapsules (MONCs) have been synthesized under similar reaction conditions and characterized by crystallographic, electrochemical, and magnetic susceptibility techniques. Both MONCs contain 24 Mn centers but, somewhat surprisingly, marked differences in oxidation state distribution are observed upon analysis. One MONC contains exclusively Mn^{II} ions, whilst the other is a mixed-valence Mn^{II}/Mn^{III} assembly. We propose that these disparate oxidation state distributions arise from slight differences in pH achieved during synthesis, a factor that may lead to many spectacular new MONCs (and associated host-guest chemistries).

INTRODUCTION

The controlled synthesis of high-nuclearity transition metal clusters is a challenging goal that continues to attract intense interest. This is primarily due to the fact that the species isolated often have exciting physical properties, an example being their ability to act as metalloenzyme models;[1-7] different metal ions and organic ligands have been combined in a variety of ways to afford such biomimetic structures.[8-14] A great deal of effort has also been invested in the systematic construction of nanoscale complexes containing paramagnetic metal ions, as these can display fascinating magnetic properties (e.g. Single-Molecule Magnets).[15-27]

In recent times our research has focused on the metal-directed assembly of *C*-alkylpyrogallol[4]arenes (PgC_n, where *n* is the number of carbon atoms in the pendant alkyl chains).[15,28-37] PgC_ns are bowl-shaped polyphenols and, upon deprotonation, their upper-rim phenolic groups may coordinate to appropriate metal ions, leading to the formation of metal-organic nanocapsules (MONCs).[15,28-31,33-38] MONCs are primarily self-assembled into two different structural forms, hexamers and dimers. In this notation, hexamers contain 6 PgC_ns and 24 metal ions in the general metal-organic cage structure, whilst dimers have 2 and 8 equivalents respectively. Over the past few years we have reported the synthesis and structural analysis of several different MONCs, some of which are assembled with mixed-valence metal centers.[15,28-31,33-37,39,40] Given this observation, we recently turned our attention to the targeted synthesis of mixed-valence MONCs via *in-situ* redox reactions.[41] In this contribution we present the synthesis and characterization of two structurally analogous Mn-seamed MONCs, $[Mn^{II}_{24}(PgC_5)_6(H_2O)_{24}]$ and $[Mn^{II}_{18}Mn^{III}_6(\mu_2\text{-}Cl)_6(\mu_3\text{-}Cl)_2(PgC_5)_6(H_2O)_{30}]$ (**1** and **2** respectively), that are formed under similar reaction conditions (Figure 1) but that display marked differences in oxidation state distribution. The presence of mixed-valence metal centers in **2** suggests the occurrence of an oxidation process taking place during self-assembly, a fact we believe is attributable to subtle differences in pH resulting during the individual reactions.

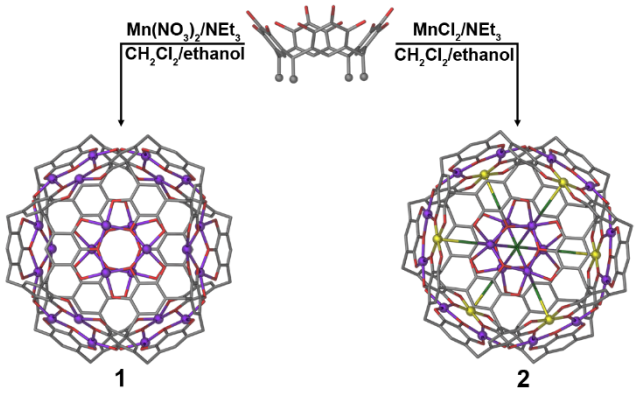

Figure 1. Reaction conditions used for the synthesis of **1** and **2**, and their symmetry expanded X-ray crystal structures. Disordered PgC_5 alkyl chains and H atoms have been removed for clarity. Color code: Mn^{II} – purple, Mn^{III} – yellow, Cl – green, C – grey, O – red.

EXPERIMENTAL SECTION

Synthesis of *C*-pentylpyrogallol[4]arene (PgC_5): Pyrogallol (25 g. 0.21 mol) was dissolved in 95% ethanol (40 ml) in a 250-ml round-bottomed flask. Hexanal (25 ml, 0.20 mol) and concentrated HCl (1 ml) was added and the mixture refluxed overnight. The resultant white crystalline product was filtered and dried under vacuum. The final product (PgC_5) was used for the synthesis of **1** and **2** without further purification.

Synthesis of 1: A 1:1 (v/v) CH_2Cl_2/ethanol mixture of PgC_5 (0.166 g, 0.2 mmol) and triethylamine (112 µl, 0.8 mmol) was sonicated for ~20 minutes at 45°C. The resulting pinkish-white turbid solution was cooled to room temperature and

$Mn(NO_3)_2.4H_2O$ (0.2002 g, 0.8 mmol) was added. The mixture was further sonicated at 45°C for 30 minutes (Final pH = 4.64), affording a black solution that was set aside. Black single crystals that were of diffraction quality were obtained over a period of 2-3 weeks. Unit cells of several crystals were checked in order to establish sample homogeneity. Yield = 0.0432 g (19 % based on Mn).

Synthesis of 2: A 1:1 (v/v) CH_2Cl_2/ethanol mixture of PgC_5 (0.166 g, 0.2 mmol), and triethylamine (112 µl, 0.8 mmol) was sonicated for ~20 minutes at 45°C. The resulting pinkish-white turbid solution was cooled to room temperature and $MnCl_2.4H_2O$ (0.1583 g, 0.8 mmol) was added. The solution was further sonicated at 45°C for 30 minutes (Final pH = 3.24), affording a brown solution that was set aside. Brown single crystals that were of diffraction quality were obtained by slow evaporation of the mother liquor over a period of two days. Unit cells of several crystals were checked in order to establish sample homogeneity. Yield = 0.0598 g (25 % based on Mn).

Characterization Techniques.

Single-crystal X-ray Diffraction Analysis: Single crystal X-ray crystallographic data of **1** and **2** were collected on Bruker Prospector CCD area detector under Cu-K_α radiation. The structures were solved and refined using SHELX programs and X-SEED. In order to handle the disorder associated with solvent molecules and model the structure appropriately, SQUEEZE program was applied to both data sets.

Electrochemistry: Electrochemical data were obtained with a Bioanalytical Systems Inc. (BASi, West Lafayette, IN) CV-50. Tetraethylammonium perchlorate (TEAP; 0.1 M) in acetonitrile (Sigma Aldrich, HPLC grade, ≥99.93%) was used as the electrolytic solution. A non-aqueous Ag/AgCl reference electrode (BASi) was used as the reference electrode, in addition to a platinum wire auxiliary electrode, and a Pt-disk working electrode. A scan rate of 100 mV s^{-1} was used for all experiments. Formal potentials were standardized against the ferrocenium (Fc^+) / ferrocene (Fc) redox couple. Under these experimental conditions, the Fc^+/Fc redox couple was observed as $E_{1/2}$ = 0.420 V vs Ag/AgCl in acetonitrile. Formal reduction potentials were calculated as the mean of the cathodic and anodic peaks. All experimental solutions were degassed with Ar(g) prior to use and the experiments were performed under a blanket of Ar(g).

Magnetism: DC magnetic susceptibility and magnetization measurements were performed on finely ground samples of compounds **1** and **2** using a Quantum Design MPMS XL SQUID magnetometer operating in the T = 2 – 300 K and H = 0 – 7 T temperature and field ranges, respectively. Diamagnetic corrections were applied to the data using Pascal's constants. The samples were prepared in a glove box and stored under N_2 prior to measurement to avoid oxidation.

RESULTS AND DISCUSSION

X-ray Crystallographic Analysis of Nanocapsules 1 and 2. Compound **1** crystallized in a trigonal cell and structure solution was carried out in the space group *R-3c*. The asymmetric unit (ASU) in **1** comprises one sixth of the MONC structure, and symmetry expansion affords the entire framework containing 24 Mn^{II} ions and 6 PgC_5 units (Figure 2a). Interestingly, the overall metal-organic arrangement of this nanocapsule is strikingly similar to that of the previously reported Zn^{II}-seamed analog.[36] On the basis of both bond-valence sum (BVS) analysis[42] and inspection of the Mn—O bond distances, all of the constituent Mn ions in **1** were determined to be in the 2+ oxidation state (Table S1). These Mn^{II} ions are disordered over two positions, in- and out of the plane of the nanocapsule surface, and they all display distorted square pyramidal geometry by coordination to four equatorial phenolic oxygen atoms and an axial aqua ligand (Figure 2b). In order to achieve a satisfactory structural model, all four unique Mn^{II} ions were refined using partial occupancies. The occupancies of three sites refined to 75%/25% while the fourth refined to 80%/20%. The presence of different levels of disorder at different sites suggests that each site on a molecule may be randomly occupied, although this slight difference does not completely rule out a scenario where the crystals contains a disordered mix of two molecules which are themselves ordered. Figure 2a shows the disordered Mn ions present in just one position (which in this case is at higher occupancy), and inspection shows two facets that are related through an inversion center. These are oriented towards the interior of the MONC, forming two concave distortions on the framework as a result. The axial water ligands on these concave sites are all located on the interior, whereas those on the other six facets are pointing away from the MONC exterior (Figure 2c).

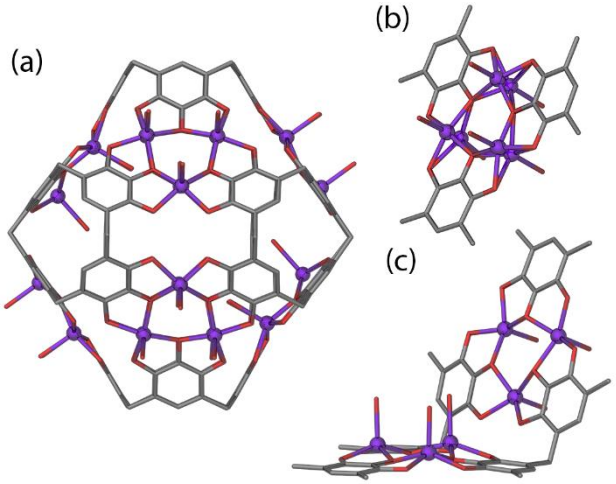

Figure 2. (a) A side view of **1** showing the arrangement of disordered metal ions at their highest occupancies. (b) Top-down view of a $[Mn_3O_3]$ cyclic array with disordered Mn^{II} ions shown in both positions. (c) Two adjacent facets of **1**, near a concave site, showing the coordination of axial water molecules to Mn^{II} ions. Disordered PgC_5 alkyl chains and H atoms have been removed for clarity. Color code: Mn^{II} – purple, C – grey, O – red.

Compound **2** was also crystallized in a trigonal cell, and structure solution was again carried out in the space group *R-3c*. Structural analysis of **2** (Figure 3a) showed that, as is the case in **1**, the framework consists of 24 Mn ions and 6 PgC_5 units with the ASU containing one sixth of the structure. Interestingly, the internal cavity of **2** contains 8 µ-Cl^- ions which serve as bridging ligands between adjacent facets in the MONC framework. Inspection of the structure of **2** shows that all Mn ions are six-coordinate, and that these display two distinct coordination environments. BVS analysis, coupled with examination of the Mn—O bond distances, reveals that all Mn ions are

in either 2+ or 3+ oxidation states (Table S2). The Mn ions in six facets are co-planar with the PgC_5 upper-rim phenolic oxygens, and these show distorted octahedral geometries by bonding to two axial ligands (Figure 3b). In these facets, each $[Mn_3O_3]$ unit consists of two Mn^{II} ions (Mn1, Mn2, and symmetry equivalents, s. e.) and one Mn^{III} ion (Mn3 and s. e.). Both Mn1 and Mn2 coordinate to four equatorial phenolic oxygen atoms, and two axial aquo ligands, whilst the Mn3 ion bonds to four equatorial phenolic oxygens, an aquo ligand on the MONC exterior, and a μ-Cl^- ion (Cl1, and s. e.) on the interior. Cl1 bridges between Mn3 and Mn^{II} ions in an adjacent facet (Mn4 and s.e., Figure 3c), and this occurs with unique Mn3—Cl1 and Mn4—Cl1 bond distances of 2.805(3) and 2.452(4) Å, respectively. The relatively long Mn3—Cl1 bond distance can be explained by Jahn-Teller elongation along the Cl1—Mn3—O3O vector, which is characteristic for Mn^{III} ions and is close to linearity with an angle of 177.9(3)°.

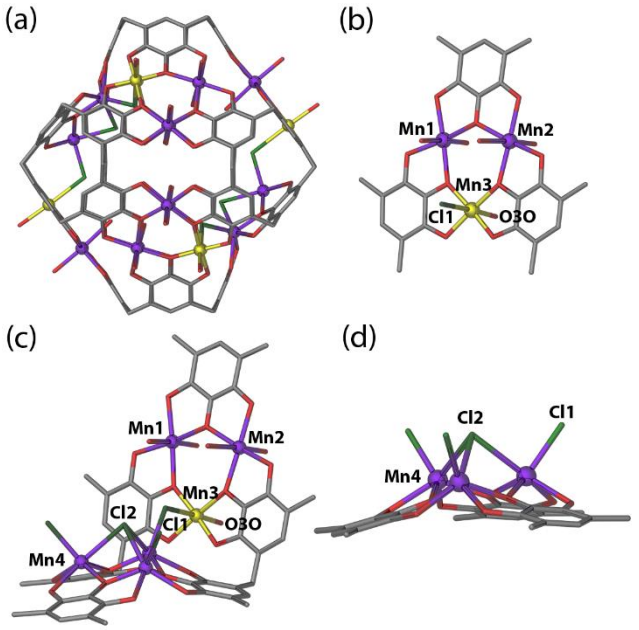

Figure 3. (a) A side view of **2** showing the metal-ligand arrangement in the framework. (b) Top-down view of a $[Mn_3O_3]$ unit showing the distorted octahedral coordination spheres around Mn^{II} and Mn^{III} ions. (c) A view of two adjacent facets near a concave site showing the coordination of μ-Cl^- ions between constituent Mn ions. (d) Coordination of μ_3-Cl^- ion (Cl2) between Mn4 ions which resulted in slight concave distortions on the framework. Disordered PgC_5 alkyl chains and H atoms have been removed for clarity. Color code: Mn^{II} – purple, Mn^{III} – yellow, Cl – green, C – grey, O – red.

Further analysis of **2** revealed that the Mn4 ions in the remaining two facets, which are related by an inversion center, show distorted trigonal prismatic geometry. As shown in Figure 3d, the coordination sphere around Mn4 consists of four upper-rim phenolic groups and two μ-Cl^- ions on the MONC interior: μ-Cl1 bridges between Mn3 and Mn4, and another μ_3-Cl^- ion (Cl2), caps all three Mn4 ions. As a result of having μ-Cl^- linkages, these two facets are bent inwards, forming slight concave distortions / dents to the framework. Interestingly, and unlike in the case of **1**, all the Mn ions in **2** are in crystallographically ordered positions, a feature likely due the anchoring nature of the μ-Cl^- ions. Further inspection revealed that, because of these internal linkages, four adjacent facets are interconnected (Figure 4) such that, as shown in Figure 1, **2** possesses a C_6 rotation axis that is coincident with both concave sites.

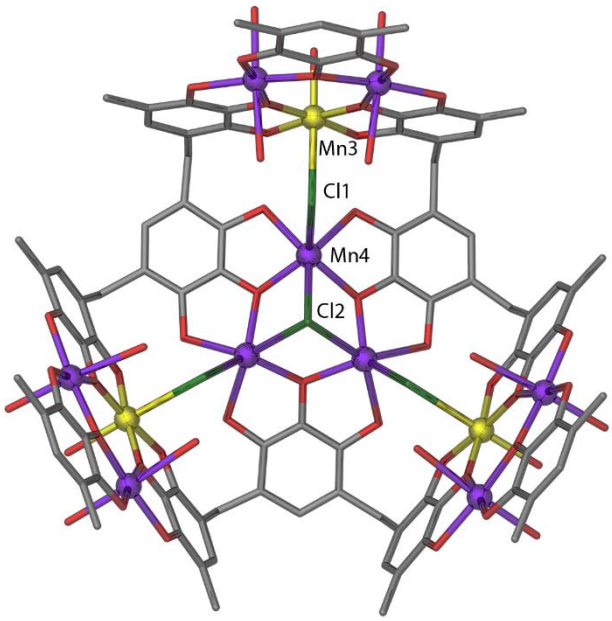

Figure 4. A top-down view of one of the concave site of **2** showing four adjacent facets are interconnected through μ-Cl linkages. Disordered PgC_5 alkyl chains and H atoms have been removed for clarity. Color code: Mn^{II} – purple, Mn^{III} – yellow, Cl – green, C – grey, O – red.

Void volumes of **1** and **2** were calculated using MSRoll with a sphere radius of 1.25 Å. Compound **1** was found to enclose a volume of ~1300 $Å^3$, and the internal volume of **2** was calculated twice: first, by including all interior μ-Cl^- linkages (1060 $Å^3$) and then, by excluding all internal axial ligands (~1340 $Å^3$). These calculated volumes clearly show that, despite possessing slight framework distortions, both MONCs possess sufficient internal space to house multiple guest molecules.

Electrochemical Analysis. We previously observed a nitrate mediated oxidation of Mn^{II} ions during the assembly of a mixed-valence MONC (**3**).[41] Since H^+ ions play an important role in nitrate reduction, NO_3^- ions act as electron acceptors only under low pH conditions.[43,44] Interestingly, the reaction conditions used in the synthesis of **3** are similar to those of **1** (Figures S3 and S4). However, the fact that the framework of **1** consists of solely Mn^{II} ions suggests that a potential redox process has possibly been prevented by a slightly higher pH value observed during synthesis (pH = 4.64). That is, during the formation of **1** and **3**, the effectiveness of NO_3^- ions to act as electron acceptors has likely been determined by the resulting pH value. With regard to **2**, similar to molecular oxygen-mediated Fe^{II} to Fe^{III} oxidation,[45,46] we propose that the framework Mn^{III} ions are

formed by aerobic oxidation of Mn^{II} ions. Based on the proposed electron transfer reaction [Eq. (1)], the resulting low pH value likely plays a key role in yielding Mn^{III} ions (pH = 3.24). In addition, the size of the Cl^- ions may have played a vital role since they are coordinated from the capsule interior. In general, these observations suggested that slight changes in reaction conditions, in this case the resulting pH value and the identity of counter anion, drastically affect the chemical activity / role of metal ions, as well as that of other reagents / components during the self-assembly process.

$$4\ Mn^{II} + 4\ H_3O^+ + O_2 \rightarrow 4\ Mn^{III} + 6\ H_2O \quad (1)$$

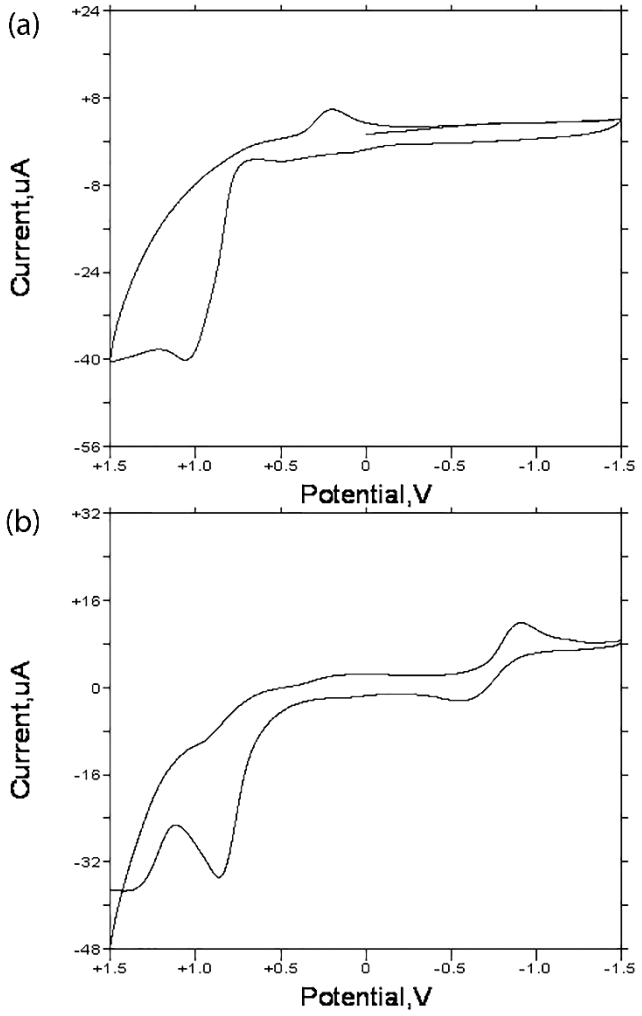

Figure 5. Cyclic voltammograms of compounds (a) **1**, and (b) **2** in acetonitrile with 0.1 M TEAP. Scan rate is 100 mV s^{-1}.

The electrochemical behavior of **1** and **2** were each studied by cyclic voltammetry in the potential window +1.5 V to -1.5 V. The cyclic voltammogram for **1** (Figure 5a) showed a single irreversible oxidation at +1.279 V consistent with Mn(II) containing species.[47-49] This peak is attributed to the oxidation process Mn^{II} to Mn^{IV} which is likely caused by molecular oxygen. Compound **2** showed electrochemical behavior consistent with previously reported mixed-valent manganese complexes (Figure 5b).[47-50] A reversible reduction is observed at -0.508 V that is attributed to the reduction process of Mn^{III} to Mn^{II}. Repetitive cyclic voltammetry scans confirmed the reversibility of the process (Figure S5). The separation between the cathodic and anodic peaks of 0.440 V is far greater than the 0.059/*n* V separation predicted for an electrochemically reversible *n*-electron process. This means the process chemically reversible but not electrochemically reversible. An irreversible oxidation is observed at +1.080 V and attributed to the process Mn^{II} to Mn^{IV}. This potential is consistent with oxidation of Mn^{II} by molecular oxygen.[47] Overall, the electrochemical activities of **1** and **2** support the fact that these nanocapsules are arranged differently during the assembly processes, and these differential arrangements considerably affect their physical properties.

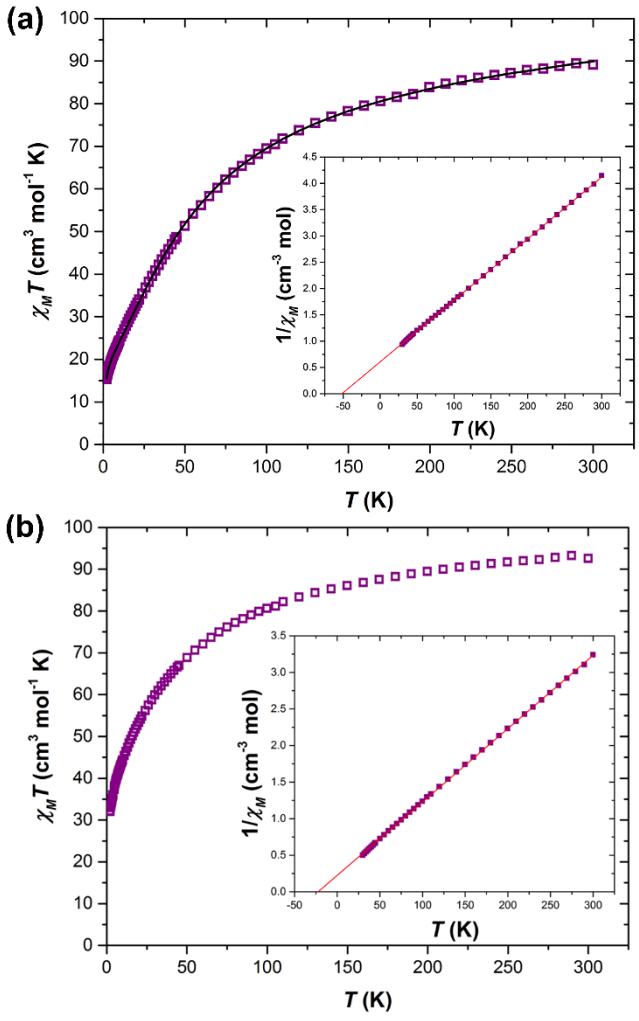

Figure 6. (a) Plot of the $\chi_M T$ product versus T for compound **1**, the solid black line is a fit of the experimental data to spin-Hamiltonian [Eq. (2)]. Inset: plot of $1/\chi_M$ versus T. The solid red line is a fit of the data to the Curie-Weiss Law. (b) Plot of the $\chi_M T$ product versus T for compound **2**. Inset: plot of $1/\chi_M$ versus T. The solid red line is a fit of the data to the Curie-Weiss Law.

Magnetic Susceptibility. Direct current (DC) magnetic susceptibility measurements were carried out on powdered polycrystalline samples of compounds **1** and **2** in an applied magnetic field H = 0.1 T over the temperature range T = 2 - 300 K. The experimental data for **1** (Figure 6a) and **2** (Figure 6b) are

plotted as the $\chi_M T$ product versus T, where χ_M is the molar magnetic susceptibility and T is the temperature. For **1**, the value of $\chi_M T$ at T = 300 K is 89.5 cm^3 K mol^{-1}, lower than that expected for the sum of the Curie constants for 24 Mn^{II} (s = 5/2) ions with g_{Mn} = 2.00 (105.0 cm^3 K mol^{-1}). With decreasing temperature, the magnitude of $\chi_M T$ gradually decreases, reaching a value of 15.3 cm^3 K mol^{-1} at T = 2 K. This behavior is indicative of the presence of (relatively weak) antiferromagnetic (AF) exchange interactions between the constituent metal ions, as would be expected for a large cluster containing multiple Mn^{II} ions.[51] Fitting the linear section of the $1/\chi_M$ versus T data (Figure 6a inset; T = 300 - 30 K) affords Curie and Weiss constants of C = 105.3 cm^3 K mol^{-1} and θ = - 51.9 K, respectively. For **2**, the value of $\chi_M T$ at T = 300 K is 93.3 cm^3 K mol^{-1}, close to the value expected for the sum of the Curie constants for 18 Mn^{II} (s = 5/2) ions and 6 Mn^{III} (s = 2) ions, with g_{Mn} = 2.00 (96.8 cm^3 K mol^{-1}). As the temperature decreases, the magnitude of $\chi_M T$ decreases reaching a value of 32.0 cm^3 K mol^{-1} at T = 2 K. This reveals the presence of weak AF exchange interactions between the metal centres. A fit of the linear section of the $1/\chi_M$ versus T data (Figure 6b inset; T = 300 - 30 K) affords Curie and Weiss constants of C = 96.2 cm^3 K mol^{-1} and θ = - 21.6 K, respectively. Magnetization (M) data collected for both **1** and **2** in the H = 0 - 7 T and T = 2 - 7 K temperature and field ranges are consistent with the presence of weak AF exchange, with the magnitude of M increasing in an almost linear fashion with increasing H without reaching saturation in both cases (Figures S6 and S7).

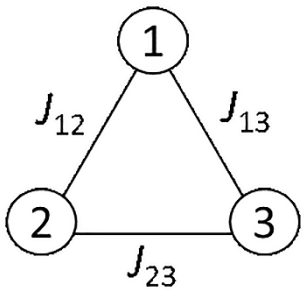

Scheme 1: Magnetic exchange interaction model employed to fit the DC susceptibility data for compound 1.

$$\hat{H} = -2J_{12}(\hat{S}_1 \cdot \hat{S}_2) - 2J_{13}(\hat{S}_1 \cdot \hat{S}_3) - 2J_{23}(\hat{S}_2 \cdot \hat{S}_3) \quad (2)$$

Compound **1** is constructed from 8 scalene [Mn^{II}_3] triangles (the ASU contains 4 independent, disordered Mn^{II} ions) with the shortest super-exchange pathway between triangles being 11 atoms in length. Assuming this pathway to be negligible allows us to employ the super-exchange model depicted in Scheme 1 and isotropic spin-Hamiltonian (2) to fit the DC susceptibility data. This afforded best fit parameters, $J_{12} = J_{23}$ = -1.31 cm^{-1} and J_{13} = -3.14 cm^{-1} (solid line in Figure 6a). These values are comparable to previously reported exchange constants for alkoxo-bridged Mn^{II} complexes where typically $J \leq |5|$ cm^{-1} and AF.[52-55] For example, in the triangular complex $[Mn^{II}_3(bpymca)_3(H_2O)_6]Cl_3$ the magnetic exchange between neighboring Mn^{II} ions is ~1.5 cm^{-1}.[51] The presence of the additional bridging chloride anions and the existence of multiple oxidation states in compound **2**, prevents any quantitative data analysis.

CONCLUSION

In conclusion, we have presented the synthesis and characterization of two Mn-seamed MONCs that display marked differences in oxidation state distribution. The presence of mixed-valence centers in one of the nanocapsules suggests the occurrence of an oxidation process during assembly, and we propose that this occurs via aerobic oxidation of Mn^{II} ions. Since both MONCs were synthesized under similar reaction conditions and given that only one comprises mixed-valence Mn centers, we propose that the progression of these *in-situ* redox reactions is, at least to some extent, influenced by the resulting pH achieved during synthesis. This discovery opens up a new realm of experimental possibilities with this incredibly versatile capsule system, and future work will investigate the effects of different factors in the promotion of *in-situ* redox reactions that drive these remarkable self-assembly processes. We anticipate that these approaches will therefore give access to a vast range of novel redox-based mixed-valence MONCs through systematic adjustment of reaction conditions. These attempts may lead to the formation of MONCs with various oxidation state distributions / compositions, thus altering the interactions between constituent metal ions, and consequently allowing for the fine-tuning of magnetic properties. We are currently undertaking further studies on introducing different anchoring / bridging ligands inside the MONC cavity. Inserting of appropriate ligands may aid the encapsulation of suitably functionalized guest species through, for example, electronic interactions, during the assembly process. Appropriately encapsulated such host-guest species will then be studied as specific biological targets or molecular electronics / magnets. Studies related to these approaches will be reported in due course.

ASSOCIATED CONTENT

Supporting Information. The Supporting material is available free of charge via the Internet at http://pubs.acs.org.
X-ray crystallography data for nanocapsules **1** (CCDC 1552756) and **2** (CCDC 1834243) (CIF).
Detailed experimental methods and crystallography data (S1-S3), Tables S1 and S2, Figures S1-S7, MALDI-TOF and DLS spectra (PDF).

AUTHOR INFORMATION

Corresponding Author

* atwoodj@missouri.edu

Author Contributions

The manuscript was written through contributions of all authors. All authors have given approval to the final version of the manuscript.

Notes

The authors declare no competing financial interest.

ACKNOWLEDGMENT

The authors thank Beverley B. DeGau for mass spectrometry analysis of this work. The authors also acknowledge the University of

Missouri Fellowship Program in Radiochemistry sponsored by US Nuclear Regulatory Commission (NRC) Grant NRC-HQ-84-15-G-0036 (J. E. Baumeister).

REFERENCES

(1) Chepelin, O.; Ujma, J.; Wu, X.; Slawin, A. M.; Pitak, M. B.; Coles, S. J.; Michel, J.; Jones, A. C.; Barran, P. E.; Lusby, P. J. *J. Am. Chem. Soc.* **2012**, *134*, 19334.

(2) Gangemi, C. M.; Pappalardo, A.; Sfrazzetto, G. T. *RSC Adv.* **2015**, *5*, 51919.

(3) Hubin, T. J.; McCormick, J. M.; Collinson, S. R.; Buchalova, M.; Perkins, C. M.; Alcock, N. W.; Kahol, P. K.; Raghunathan, A.; Busch, D. H. *J. Am. Chem. Soc.* **2000**, *122*, 2512.

(4) Kishi, N.; Akita, M.; Yoshizawa, M. *Angew. Chem. Int. Ed.* **2014**, *53*, 3604.

(5) Rulíšek, L. r.; Vondrášek, J. *J. Inorg. Biochem.* **1998**, *71*, 115.

(6) Vallee, B. L.; Williams, R. *Proc. Natl. Acad. Sci. U.S.A.* **1968**, *59*, 498.

(7) Yin, G.; Danby, A. M.; Kitko, D.; Carter, J. D.; Scheper, W. M.; Busch, D. H. *J. Am. Chem. Soc.* **2007**, *129*, 1512.

(8) Caulder, D. L.; Raymond, K. N. *Acc. Chem. Res.* **1999**, *32*, 975.

(9) Granzhan, A.; Riis-Johannessen, T.; Scopelliti, R.; Severin, K. *Angew. Chem. Int. Ed.* **2010**, *49*, 5515.

(10) Gu, Z. Y.; Park, J.; Raiff, A.; Wei, Z.; Zhou, H. C. *ChemCatChem* **2014**, *6*, 67.

(11) Kishi, N.; Li, Z.; Yoza, K.; Akita, M.; Yoshizawa, M. *J. Am. Chem. Soc.* **2011**, *133*, 11438.

(12) McKinlay, R. M.; Atwood, J. L. *Angew. Chem. Int. Ed.* **2007**, *46*, 2394.

(13) Sénèque, O.; Rager, M.-N.; Giorgi, M.; Reinaud, O. *J. Am. Chem. Soc.* **2000**, *122*, 6183.

(14) Zhao, M.; Ou, S.; Wu, C.-D. *Acc. Chem. Res.* **2014**, *47*, 1199.

(15) Atwood, J. L.; Brechin, E. K.; Dalgarno, S. J.; Inglis, R.; Jones, L. F.; Mossine, A.; Paterson, M. J.; Power, N. P.; Teat, S. J. *Chem. Commun.* **2010**, *46*, 3484.

(16) Brechin, E. K. *Chem. Commun.* **2005**, 5141.

(17) Lis, T. *Acta Crystallogr. Sect. B* **1980**, *36*, 2042.

(18) Manoli, M.; Collins, A.; Parsons, S.; Candini, A.; Evangelisti, M.; Brechin, E. K. *J. Am. Chem. Soc.* **2008**, *130*, 11129.

(19) Mitchell, S. G.; Molina, P. I.; Khanra, S.; Miras, H. N.; Prescimone, A.; Cooper, G. J. T.; Winter, R. S.; Brechin, E. K.; Long, D.-L.; Cogdell, R. J.; Cronin, L. *Angew. Chem. Int. Ed.* **2011**, *50*, 9154.

(20) Mukhopadhyay, S.; Mandal, S. K.; Bhaduri, S.; Armstrong, W. H. *Chem. Rev.* **2004**, *104*, 3981.

(21) Murugesu, M.; Habrych, M.; Wernsdorfer, W.; Abboud, K. A.; Christou, G. *J. Am. Chem. Soc.* **2004**, *126*, 4766.

(22) Neves, A.; de Brito, M. A.; Vencato, I.; Drago, V.; Griesar, K.; Haase, W. *lnorg. Chem.* **1996**, *35*, 2360.

(23) Sessoli, R.; Gatteschi, D.; Caneschi, A.; Novak, M. A. *Nature* **1993**, *365*, 141.

(24) Sessoli, R.; Tsai, H. L.; Schake, A. R.; Wang, S.; Vincent, J. B.; Folting, K.; Gatteschi, D.; Christou, G.; Hendrickson, D. N. *J. Am. Chem. Soc.* **1993**, *115*, 1804.

(25) Taylor, S. M.; McIntosh, R. D.; Piligkos, S.; Dalgarno, S. J.; Brechin, E. K. *Chem. Commun.* **2012**, *48*, 11190.

(26) Taylor, S. M.; McIntosh, R. D.; Reze, J.; Dalgarno, S. J.; Brechin, E. K. *Chem. Commun.* **2012**, *48*, 9263.

(27) Taylor, S. M.; Sanz, S.; McIntosh, R. D.; Beavers, C. M.; Teat, S. J.; Brechin, E. K.; Dalgarno, S. J. *Chem. Eur. J.* **2012**, *18*, 16014.

(28) Dalgarno, S. J.; Power, N. P.; Atwood, J. L. *Chem. Commun.* **2007**, 3447.

(29) Fowler, D. A.; Mossine, A. V.; Beavers, C. M.; Teat, S. J.; Dalgarno, S. J.; Atwood, J. L. *J. Am. Chem. Soc.* **2011**, *133*, 11069.

(30) Fowler, D. A.; Rathnayake, A. S.; Kennedy, S.; Kumari, H.; Beavers, C. M.; Teat, S. J.; Atwood, J. L. *J. Am. Chem. Soc.* **2013**, *135*, 12184.

(31) Jin, P.; Dalgarno, S. J.; Atwood, J. L. *Coord. Chem. Rev.* **2010**, *254*, 1760.

(32) Kumari, H.; Kline, S. R.; Dennis, C. L.; Mossine, A. V.; Paul, R. L.; Deakyne, C. A.; Atwood, J. L. *Angew. Chem. Int. Ed.* **2012**, *51*, 9263.

(33) McKinlay, R. M.; Cave, G. W. V.; Atwood, J. L. *Proc. Natl. Acad. Sci. U.S.A.* **2005**, *102*, 5944.

(34) McKinlay, R. M.; Thallapally, P. K.; Atwood, J. L. *Chem. Commun.* **2006**, 2956.

(35) Power, N. P.; Dalgarno, S. J.; Atwood, J. L. *New J. Chem.* **2007**, *31*, 17.

(36) Rathnayake, A. S.; Barnes, C. L.; Atwood, J. L. *Cryst. Growth Des.* **2017**, *17*, 4501.

(37) Rathnayake, A. S.; Feaster, K. A.; White, J.; Barnes, C. L.; Teat, S. J.; Atwood, J. L. *Cryst. Growth Des.* **2016**, *16*, 3562.

(38) Jin, P.; Dalgarno, S. J.; Barnes, C.; Teat, S. J.; Atwood, J. L. *J. Am. Chem. Soc.* **2008**, *130*, 17262.

(39) Dalgarno, S. J.; Power, N. P.; Atwood, J. L. *Coord. Chem. Rev.* **2008**, *252*, 825.

(40) Jin, P.; Dalgarno, S. J.; Warren, J. E.; Teat, S. J.; Atwood, J. L. *Chem. Commun.* **2009**, 3348.

(41) Rathnayake, A. S.; Fraser, H. W. L.; Brechin, E. K.; Dalgarno, S. J.; Baumeister, J. E.; White, J.; Rungthanaphatsophon, P.; Walensky, J. R.; Barnes, C. L.; Teat, S. J.; Atwood, J. L. *Nat. Commun.* **2018**, *9*, 2119.

(42) Brown, I.; Altermatt, D. *Acta Cryst. B* **1985**, *41*, 244.

(43) Huang, C.-P.; Wang, H.-W.; Chiu, P.-C. *Water Res.* **1998**, *32*, 2257.

(44) Huang, Y. H.; Zhang, T. C. *Water Res.* **2004**, *38*, 2631.

(45) Feig, A. L.; Lippard, S. J. *Chem. Rev.* **1994**, *94*, 759.

(46) Nordstrom, D. K.; Alpers, C. N.; Ptacek, C. J.; Blowes, D. W. *Environ. Sci. Technol.* **2000**, *34*, 254.

(47) Belal, A. A.; Chaudhuri, P.; Fallis, I.; Farrugia, L. J.; Hartung, R.; MacDonald, N. M.; Nuber, B.; Peacock, R. D.; Weiss, J.; Weighardt, K. *lnorg. Chem.* **1991**, *30*, 4397.

(48) Cooper, S. R.; Calvin, M. *J. Am. Chem. Soc.* **1977**, *99*, 6623.

(49) Morrison, M. M.; Sawyer, D. T. *lnorg. Chem.* **1978**, *17*, 333.

(50) Saalfrank, R. W.; Scheurer, A.; Prakash, R.; Heinemann, F. W.; Nakajima, T.; Hampel, F.; Leppin, R.; Pilawa, B.; Rupp, H.; Müller, P. *lnorg. Chem.* **2007**, *46*, 1586.

(51) Perea-Buceta, J. E.; Mota, A. J.; Costes, J.-P.; Sillanpää, R.; Krzystek, J.; Colacio, E. *Dalton Trans.* **2010**, *39*, 10286.

(52) Sakiyama, H.; Kato, M.; Sasaki, S.; Tasaki, M.; Asato, E.; Koikawa, M. *Polyhedron* **2016**, *111*, 32.

(53) Wesolek, M.; Meyer, D.; Osborn, J. A.; De Cian, A.; Fischer, J.; Derory, A.; Legoll, P.; Drillon, M. *Angew. Chem. Int. Ed.* **1994**, *33*, 1592.

(54) Zhao, L.; Xu, Z.; Grove, H.; Milway, V. A.; Dawe, L. N.; Abedin, T. S.; Thompson, L. K.; Kelly, T. L.; Harvey, R. G.; Miller, D. O. *lnorg. Chem.* **2004**, *43*, 3812.

(55) Huang, D.; Wang, W.; Zhang, X.; Chen, C.; Chen, F.; Liu, Q.; Liao, D.; Li, L.; Sun, L. *Eur. J. Inorg. Chem.* **2004**, *2004*, 1454.

Insert Table of Contents artwork here